# Pressure dependence of the configurational bistability and deep electronic levels of the MFe center in InP

G. A. Samara
*Sandia National Laboratories, Albuquerque, New Mexico 87185, USA*

C. E. Barnes
*Jet Propulsion Laboratory, California Institute of Technology, Pasadena, California 91109, USA*
(Received 3 November 2005; revised manuscript received 24 March 2006; published 25 April 2006)

The influence of hydrostatic pressure on the structural bistability and electronic properties of the processing-induced MFe center in Fe-doped *n*-type InP was investigated. Earlier work has shown that, when occupied by electrons, the center can be reversibly placed in either of two configurations, termed *A* and *B*, by the proper choice of electric biasing conditions and temperature. Pressure strongly modifies the energetics and kinetics of the various electronic transitions and of the transformations associated with the center. The activation volumes ($\Delta V^*$) for these processes were determined. In the absence of barriers to electron capture, or for small barriers, $\Delta V^*$ can be interpreted as the breathing mode relaxation associated with electron emission or capture. At pressures $\geqslant$8 kbar, the center exists only in the *A* configuration regardless of bias conditions, because at these pressures the energetics and kinetics of the various processes have changed so much as to always favor the *A* configuration. It is also shown that, whereas the $A \rightleftarrows B$ transformations are charge state controlled at 1 bar, this is not the case at high pressure where the transformations can be brought about without electron emission or hole capture. Earlier tentative atomic models for the center are discussed, and it is shown that some features of one of the models including the signs of the breathing mode relaxations associated with the various electron emissions are consistent with the experimental results, but issues remain. The results are also found to be generally consistent with first-principles calculations on defects in InP, but it is emphasized that whereas these calculations are for simple defects, the defects associated with the MFe center are more complex.

DOI: 10.1103/PhysRevB.73.155206 PACS number(s): 71.55.Eq

## I. INTRODUCTION

One of the more interesting and important developments in the study of lattice defects and their associated deep electronic levels in covalent semiconductors has been the discovery that an ever-increasing number of important defects exhibit configurational bistability (or multistability). Configurationally bistable defects are defects that for the same charge state can exist in two different configurations with distinct electronic and optical properties. Reversible transformations between the two configurations can be induced by thermal, electrical, or optical means, and the configuration, which is observed experimentally, is dependent on the thermal, electronic, and optical history of the sample. Examples of such configurationally bistable defects include the M-center in irradiated *n*-InP,[1] the MFe-center in Fe-doped *n*-InP,[2] the oxygen vacancy related defect in Si,[3] the boron-vacancy complex in Si,[4] and the EL2 center InGaAs.[5]

Although the properties of several configurationally bistable defects have been characterized in considerable detail, much remains to be learned about the atomic structure of the configurations and the nature of the transformations between them. The bistability is undoubtedly a manifestation of strong electron-lattice interactions, and large lattice relaxations are believed to be involved.[2,5]

In earlier work[6] we gained new insights into the physics and lattice relaxations associated with defects in semiconductors from high-pressure studies of the deep levels produced by these defects. Such studies should be extremely useful for understanding configurational bistability because with pressure we can continuously and delicately tune the strength of the electron-lattice interactions and thereby modify the balance of forces that determine the stability and nature of the different configurations.

In the present work, we have investigated the effects of hydrostatic pressure on the properties and bistability of the deep MFe center in iron (Fe) doped, *n*-type indium phosphide (InP). This center, which is presumably produced during high-temperature processing,[2] is scientifically challenging and technologically important because Fe is a widely used dopant for semi-insulating InP substrates used in fabricating group III-V compound semiconductor devices. The bistability of this center was discovered and characterized in detail at atmospheric pressure (1 bar or $\cong$0 kbar) by Levinson *et al.*[2] When occupied by electrons, the center can be reversibly placed in either of two configurations, termed *A* and *B*, by the proper choice of electric biasing conditions and temperature. The general features of this bistability will be summarized in Sec. III A. We have found that pressure has a very strong influence on the balance between these two configurations. Specifically, pressure favors the *A* over the *B* configuration, and for pressures $\geqslant$8 kbar essentially only the *A* configuration is observed. This result, along with detailed studies of the effects of pressure on the energetics of the two configurations and on the kinetics of the $B \rightarrow A$ transformation, provide important new insights into the nature of the two configurations and their associated deep levels. The results are discussed in terms of possible atomic models for the

 

*A* and *B* configurations of the MFe center. These models, referred to as Model I and Model II in our later discussion, were proposed and discussed briefly by Wager and Van Vechten,[7] who further suggested that it may be possible "to distinguish between them by experiments at high pressure." Although it will be shown that some of our results favor Model I, it cannot be said that this model has been proven, and in fact many issues and concerns about both models remain (as discussed in Sec. III G).

Section II provides a brief account of the experimental details. The results are presented and discussed in Sec. III. The paper closes with a summary and concluding remarks in Sec. IV.

## II. EXPERIMENTAL DETAILS

The samples[8] were fabricated from lightly Fe-doped, liquid encapsulated, Czochralski grown *n*-type InP with a room-temperature free-electron density of approximately $2 \times 10^{15}$ cm$^{-3}$. Mesa $p^+/n$ junction structures were formed using Zn-doped $p^+$ liquid phase epilayers.

For measurements under pressure, the samples were placed in a hydrostatic pressure apparatus which uses helium as the pressure-transmitting medium. The apparatus is capable of pressures to 10 kbar over a temperature range from 4 K to approximately 450 K. Shielded electrical leads were brought out of the pressure cell to a Sula deep-level transient spectroscopy (DLTS) spectrometer. During the DLTS scan the heating rate was controlled by a computer that also provided data processing of the output signal from the spectrometer. As we will point out later, it was necessary to determine Arrhenius plots with a great deal of precision in order to detect sometimes relatively small pressure-induced changes in emission rates and activation energies. Under such conditions, the transients were recorded at constant temperature directly from the pre-amp output of the spectrometer on a storage oscilloscope for computer processing. Capacitance-voltage (*C-V*) and thermally stimulated capacitance (TSCAP) measurements were also made with the samples under pressure using a computer-controlled system based on a HP 4275A LCR meter.

## III. RESULTS AND DISCUSSIONS

### A. Properties of the MFe center at 1 bar

Before proceeding with the pressure results, it is helpful to briefly summarize the properties of the MFe center at 1 bar. These properties were determined from thermally stimulated capacitance (TSCAP) and DLTS measurements. The main features can best be appreciated with reference to the 1 bar TSCAP spectra in Fig. 1 and DLTS spectra in Fig. 2. These spectra are taken from our work, but are very similar to those of Levinson *et al.*[2] The features are as follows.

(i) When occupied by electrons, the MFe center can exist in either the *A* or *B* configurations (following Levinson *et al.*'s nomenclature). Configuration *A* is obtained by cooling the sample with no applied bias, i.e., in the presence of free electrons, whereas configuration *B* is obtained by cooling under reverse bias, i.e., in the absence of free carriers, followed by removal of the bias to fill the traps.

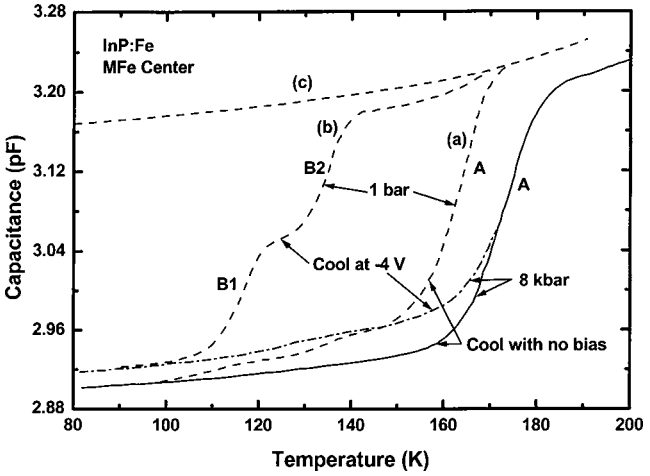


FIG. 1. Thermally stimulated capacitance (TSCAP) spectra for the *A* and *B* configurations of the MFe center in InP at 1 bar and 8 kbar. Curve (a) is obtained by cooling and subsequently heating the sample with zero bias and corresponds to configuration *A* at 1 bar. For curve (b) the sample is cooled under reverse bias (−4 V) and then heated at zero bias to yield configuration *B*. Curve (c) corresponds to the temperature dependence of the capacitance of the junction in the absence of carrier trapping. Configuration *A* is stabilized at high pressure (8 kbar scans) regardless of bias.

(ii) Curves (a) and (b) in the TSCAP spectra in Fig. 1 correspond to configurations *A* and *B*, respectively, whereas curve (c) corresponds to the temperature dependence of the capacitance of the junction in the absence of carrier trapping effects. Curve (b) consists of two main emission steps labeled *B*1 and *B*2, each presumably corresponding to the emission of one electron, whereas curve (a) has only one main step, labeled *A* (or *A*1*A*2 in Levinson *et al.*'s work). The step heights are such that $B1 \approx B2 \approx \frac{1}{2}A$. It has been noted[2] that the (a) and (b) spectra evidently arise from the same defect because the configurational transformation from *A* to *B* yields equal increases in step heights *B*1 and *B*2 and

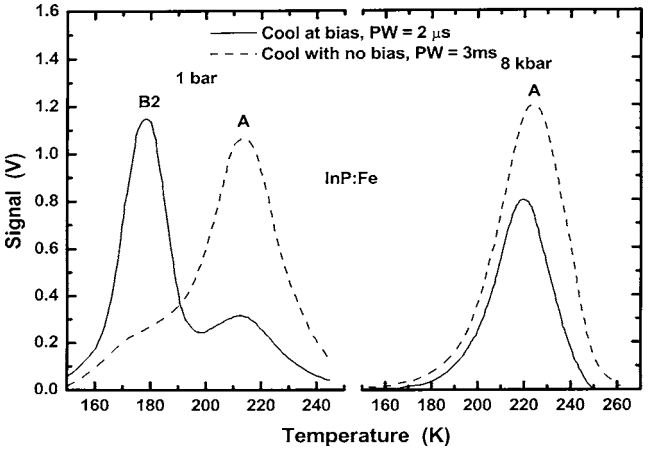


FIG. 2. DLTS spectra for the *A* and *B* configurations of the MFe center in InP at 1 bar and 8 kbar. The *B*1 transition is not seen for the conditions of this experiment. The *A* configuration is stabilized at high pressure regardless of bias (8 kbar scans).

a proportional decrease in step height $A$. The reverse is true for the $B \rightarrow A$ transformation.

One noticeable feature in the spectra is the separation between the (a) and (b) curves at low temperatures ($<100$ K) and the high temperature ($>140$ K) residual step in the (b) curve above the $B2$ transition. Levinson *et al.*[2] believed that these features may be artifacts due to the depletion-layer-edge region. While this may be a viable explanation, it is tempting to speculate that the residual step above $B2$ may implicate the involvement of a third electron in the $B \rightarrow A$ transformation. The motivation for this speculation derives from Model I alluded to above, but it is by no means certain.

(iii) The DLTS spectra in Fig. 2 exhibit peaks that correspond to the TSCAP steps in Fig. 1. In interpreting these spectra, it is important to emphasize a distinction between DLTS and TSCAP measurements. TSCAP is a single transient method in which the traps are filled only at low temperature. In contrast, in the DLTS technique, the sample is repetitively pulsed to fill the traps as the sample is heated. Under such conditions, configurational transitions between $A$ and $B$ can take place during the DLTS measurement. Levinson *et al.*[2] have expressed the steady-state fraction of centers in the $A$ configuration, $f_A$, during a DLTS scan as follows:

$$f_A = 1 - f_B = [1 - \exp(-R_{BA}t_P)][1 - \exp(-R_{AB}t_i - R_{BA}t_P)]^{-1}, \quad (1)$$

where $f_B$ is the fraction in the $B$ configuration, $R_{BA}$ and $R_{AB}$ are the transformation rates, $t_P$ is the trap filling pulse width, and $t_i$ is the time interval between pulses (=pulse width PW in the figures) determined by the frequency. Thus, the differing pulse widths indicated in Fig. 2 were used to maximize the number of centers in each configuration. Note that the pulse width required to populate the $A$ configuration is orders of magnitude larger than that for the $B$ configuration. Under either pulse condition, one can expect to reach steady state during the measurement of $B2$ and $A$ emissions because the heating rate is slow compared with the time required to reach configurational equilibrium. However, this is not true at the lower temperatures at which $B1$ would be observed ($\sim 150$ K in Fig. 2). As suggested by the data in Fig. 2, the $B1$ trap peak is either absent or very weak in a typical majority carrier DLTS scan; however, $B1$ is clearly revealed when the trap-filling pulse injects holes (20 mA forward current) into the depletion region as shown in Fig. 3. Note that the $A$ configuration is very lightly populated at 1 bar under the conditions (PW=2 $\mu$s) of the experiment in Fig. 3.

(iv) The $A \rightarrow B$ configurational transformation is charge state controlled. For the defect in configuration $A$, hole capture yields the same result as electron emission, although by a different kinetic process. Both processes result in the $B$ configuration, which captures electrons that are subsequently reemitted upon warm-up as $B1$ and $B2$. The hole-induced transformation is athermal even at low temperatures (e.g., 35 K), whereas the electron emission process is thermally activated.[2] The emission step $A$, which controls the energetics and kinetics of the $A \rightarrow B$ transformation, has an activation energy (or enthalpy) =0.39 eV (corrected for the $T^2$ dependence of the prefactor) and a large electron-capture cross section, $\sigma_\infty = 1.8 \times 10^{-14}$ cm$^2$. Levinson *et al.*[2] reported values of 0.41 eV and $1.9 \times 10^{-14}$cm$^2$ for these two values.

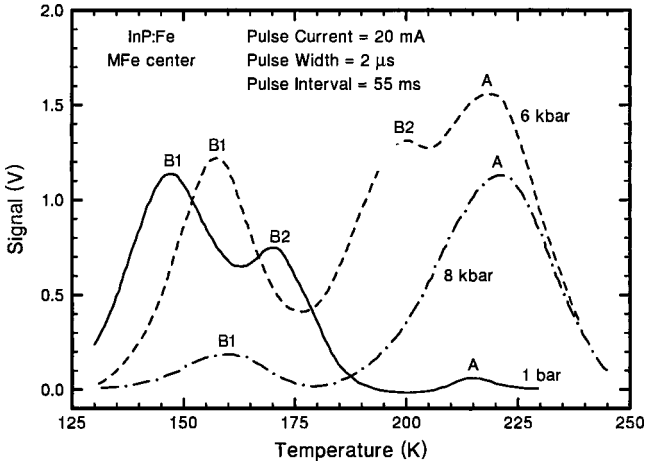


FIG. 3. DLTS spectra for the $A$ and $B$ configurations of the MFe center in InP under forward bias at 1 bar, 6 kbar, and 8 kbar. The $B1$ transition is revealed under forward bias (compare to Fig. 2). Note the merging of the $B2$ transition into the $A$ transition with pressure. The $A$ configuration is very lightly populated at 1 bar for the conditions of this experiment but becomes dominant at 8 kbar, at which pressure the $B2$ configuration has vanished.

(v) The electron thermal emission rate for $B2$ and the $B \rightarrow A$ configuration transformation rate follow Arrhenius laws. From their results, Levinson *et al.*[2] concluded that "the kinetics for the two processes are identical within experimental error" with an activation energy of 0.35 eV (not including the $T^2$ correction for $B2$) and a preexponential factor of $2.8 \times 10^{11}$ s$^{-1}$. They noted that "this finding is more remarkable when it is remembered that these two processes are in principle very different." This observation, that one configurational barrier provides the rate-limiting step for both the $B2$ emission and the $B \rightarrow A$ transformation, played an important role in Levinson *et al.*'s proposed configurational-coordinate diagram for the MFe center. As we shall see later, the pressure results make it absolutely clear that the two processes exhibit different activation energies and kinetics. The near degeneracy of these properties at 1 bar is strictly coincidental and can be removed by including the $T^2$ correction for $B2$.

(vi) The $B1$ emission is thermally activated with an activation energy of 0.27 eV (versus 0.24 eV by Levinson *et al.*[2]) and a capture cross section of $\sigma_\infty = 2.9 \times 10^{-14}$ cm$^2$.

(vii) Photoionization for configuration $A$ is not observed for $\sim 0.5 < h\nu < 1.2$ eV, and thus no $A \rightarrow B$ transformation is detected in this photon energy range.[2] [Above band gap (1.35 eV) excitation of course produces holes that promote the $A \rightarrow B$ transformation as noted in item (ii) above.] The fact that the optical ionization energy is apparently more than three times the thermal activation energy for the $A$ emission (0.39 eV) suggests that a large lattice relaxation, or Franck-Condon shift, is associated with the $A \rightarrow B$ transformation.

(viii) Photoionization was observed[2] for the $B1$ transition at $h\nu \approx 0.6$ eV. This energy is significantly larger than the thermal activation energy, suggesting that substantial lattice relaxation is associated with this transition as well. The op-

tical $B2$ transition does not induce the $B \rightarrow A$ transformation, emphasizing the thermally activated nature of the transformation process.

### B. Pressure-induced changes in the TSCAP spectra

Dramatic changes in the TSCAP spectra occur with increasing pressure, culminating at 8 kbar in the data shown in Fig. 1. Independent of the bias placed on the junction during cool down, at 8 kbar the MFe centers remain in the $A$ configuration except for small, residual amount in the $B$ state. Thus at 8 kbar the $A$ to $B$ transition rate is very small, and it is not possible to place a significant number of the MFe centers in the $B$ configuration. Note that this pressure-induced effect is significant, being much larger in a qualitative sense than typical hydrostatic pressure effects on the properties of semiconductors.[6] It should also be noted from the results in Fig. 1 that pressure shifts the $A$ emission step to higher temperatures. At 8 kbar the shift is $\sim$12 K. As we shall see later, this effect results from an increase in the $A$ trap depth.

### C. Pressure-induced changes in the DLTS spectra

The left-hand side of Fig. 2 shows the 1 bar DLTS spectra for the $A$ and $B$ configurations taken under majority carrier injection. The reverse bias was 4 V and the filling pulse was 4 V. The filling pulse widths are shown in the figure. The $B1$ spectrum is not seen in these scans, but it becomes prominent under forward bias injection (20 mA) as shown in Fig. 3. The main features of these spectra are similar to those of Levinson *et al.*,[2] but there are also some quantitative differences in the intensities of the various peaks. For the electrical conditions of the experiments in Figs. 2 and 3 and for a variety of other conditions examined, we note that the $B2$ and $A$ intensities are comparable in Fig. 2, and the intensity of $B1$ is about twice as large as $B2$ in Fig. 3. Levinson *et al.* observed that their DLTS intensities were such that $B1 \approx B2 \approx \frac{1}{2}A$ for the conditions of their experiments. It may be that our conditions were not optimum for maximum intensities for the $A$ and $B$ scans. On the other hand, Levinson *et al.* used reverse bias of 10 V (versus 4 V in our work), so there is a large $E$ field in the junction. This could certainly influence the emission rates.

Under pressure, the DLTS spectra reveal changes which mimic the changes seen in the TSCAP spectra. The 8-kbar results on the right-hand side of Fig. 2 show that cooling with the reverse bias on, which should normally set the MFe centers in the $B$ configuration, reveals only the $A$ configuration upon warming the sample to perform the scan. Similar results are shown in Fig. 3, where we also observe a prominent $B1$ peak due to hole injection. Note that even under the optimum conditions for $A \rightarrow B$ transformation, including a narrow filling pulse width (2 $\mu$s) appropriate for maximizing $B$, nearly all the defects are in the $A$ configuration at 8 kbar. We also note that both the $B1$ and $A$ peaks shift to higher temperatures with pressure (see Sec. III D below).

The 6-kbar scan in Fig. 3 is typical of pressures intermediate between 1 bar and 8 kbar in that a mixture of the two configurations is observed, even under conditions (20 mA forward bias injection and 2 $\mu$s pulse width) that should give the maximum number of centers in the $B$ configuration. At 6 kbar, the $A$ configuration has a greater population than the $B$ configuration while at 4 kbar (not shown) approximately $\frac{2}{3}$ of the centers are in the $B$ configuration. The results in Fig. 3 show that the $B2$ peak shifts much more rapidly with pressure than does the $B1$ peak. As we shall show later (Sec. III D), these differences are due mainly to pressure-induced changes in the electron emission energies.

The merging of $B2$ with $A$ as the pressure is raised shown in Fig. 3 illustrates the importance of performing both DLTS and TSCAP at several pressures. Without TSCAP results such as those in Fig. 1, it would not be clear from only a limited number of DLTS scans like the 8 kbar spectrum in Fig. 3 whether the dominant peak near 220 K at high pressure was due to $A$ or to $B2$. Careful examination of all the data, however, leads to the unequivocal conclusion that at 8 kbar, very few of the MFe centers are in the $B$ configuration, no matter what the bias or pulse conditions are during cooling and warm-up. This conclusion was further substantiated by examining several segments of the capacitance transients themselves at 8 kbar and finding only energy values equal to that for the $A$ emission.

As noted above, one means of promoting the $A \rightarrow B$ transformation at 0 kbar is by hole injection and capture by the $A$ configured MFe centers. We also find this to be the case even at 4 kbar, where about $\frac{2}{3}$ of the $A$ configuration convert to the $B$ configuration at 80 K. However, $A \rightarrow B$ conversion via capture of injected holes does not occur at 8 kbar in the temperature range we have investigated (80 K to room temperature). Thus, while the mechanism for $A \rightarrow B$ transformation at 1 bar appears to be charge state controlled[2] (electron emission or hole capture by $A$), this mechanism is not operative at $\geqslant$8 kbar. At these pressures the energetics and the kinetics of the various processes have changed so much as to always favor the $A$ configuration. We shall come back to this point below.

### D. Effects of pressure on the electron thermal emission rates, energies, and capture cross sections for the $A$, $B1$, and $B2$ deep levels

The $A$, $B1$, and $B2$ deep levels associated with the MFe center are located in the upper half of the InP band gap, and the observed electron emission is from these deep levels to the conduction-band edge, $E_c$. General detailed balance considerations relating thermal emission and capture rates for deep levels yield the following expression[6] for the thermal electron emission rate, $e_n$:

$$e_n = \sigma_n \langle v_n \rangle N_c \exp(-\Delta G_n/kT), \tag{2a}$$

$$= \sigma_n \langle v_n \rangle N_c \exp(\Delta S_n/k) \exp(-\Delta H_n/kT), \tag{2b}$$

where $\sigma_n$ is the electron capture cross section, $\langle v_n \rangle$ is the average electron thermal velocity, $N_c$ is the effective density of states in the conduction band, and $\Delta G_n (= \Delta H_n - T\Delta S_n)$ is the change in the Gibbs free energy which accompanies the emission of the electron from the deep level.

Equation (2b) can be rewritten as

$$e_n = \Lambda \exp(-\Delta H_n/kT), \tag{3}$$

where

$$\Lambda = \sigma_n \langle v_n \rangle N_c \exp(\Delta S_n/k). \tag{4}$$

In Eqs. (2)–(4), $\Delta S_n$ and $\Delta H_n$ are the total entropy and enthalpy changes accompanying electron emission. $\Delta S_n$ is the sum of the changes in entropy due to electronic degeneracy and to atomic vibrational/configurational changes.

In interpreting the temperature and pressure dependences of $e_n$, we note the following. The thermal velocity is given by $\langle v_n \rangle = (3kT/m_n^*)^{1/2}$, where $m_n^*$ is the electron effective mass ($=0.08m_e$ for InP). The density of states $N_c$ is given by $N_c = 2M_c(m_n^* kT/2\pi\hbar^2)^{3/2}$, where $M_c$ is the number of equivalent minima in the conduction band. Thus, the product $\langle v_n \rangle N_c$ is proportional to $m_n^* T^2$. The pressure dependence of $m_n^*$ in InP as well as in other semiconductor is very weak ($d \ln m_n^*/dP$), being on the order of $10^{-3}$ per kbar.[6,9] As we shall see later, this effect is negligibly small compared to the pressure dependence of $e_n$. Thus, to a good approximation for the present case we can neglect the small pressure dependence of the product $\langle v_n \rangle N_c$. We also assume that capture barriers, if present, and their pressure dependences are much smaller than the associated $\Delta H$'s and their pressure dependences, which are very large, in fact unusually so for the MFe center. This is generally found to be a reasonable assumption,[6] and any uncertainty related to it should not materially affect the conclusion drawn.

On the basis of the above considerations, we thus see that the slope in a $\ln(e_n/T^{-2})$ versus $T^{-1}$ Arrhenius plot is simply $\Delta H_n$ and that such plots at different pressures yield the pressure dependences of $\Delta H_n$. The intercepts of such plots yield $\Lambda$ and its pressure dependence which is, to a good approximation, given by

$$d \ln \Lambda/dP \cong d \ln \sigma_n/dP + k^{-1}(d\Delta S_n/dP). \tag{5}$$

On the other hand, measurements of $e_n$ versus pressure ($P$) at constant $T$ yield the pressure dependences of $\Delta G_n$ and $\sigma_n$, since from Eq. (2a) and the above considerations we have

$$(\partial \ln e_n/\partial P)_T \cong (\partial \ln \sigma_n/\partial P)_T - (kT)^{-1}(\partial \Delta G_n/\partial P)_T. \tag{6}$$

Knowing the pressure dependences of $e_n$, $\Delta H_n$, and $\Lambda$ thus allows determination of the pressure dependences of $\sigma_n$, $\Delta S_n$, and $\Delta G_n$.

Accurate emission rates were obtained from capacitance transients recorded at many fixed temperatures. For each of the levels, the conditions were set to maximize the number of MFe centers in the configuration of interest. Typical Arrhenius plots of $\log(e_n/T^2)$ versus $T^{-1}$ for the three levels are shown in Fig. 4. It was not possible to obtain data for the $B2$ trap at 8 kbar because, as noted above, it is not possible to populate this level at this pressure. In all cases $e_n$ decreases with pressure at constant temperature, and the Arrhenius plots shift to the left. Reminiscent of the spectra in Fig. 3, note that the shift of the $B2$ curves is significantly larger than the shifts of the $B1$ and $A$ curves. The observed effects are associated with pressure-induced changes in $\Delta H_n$ and the

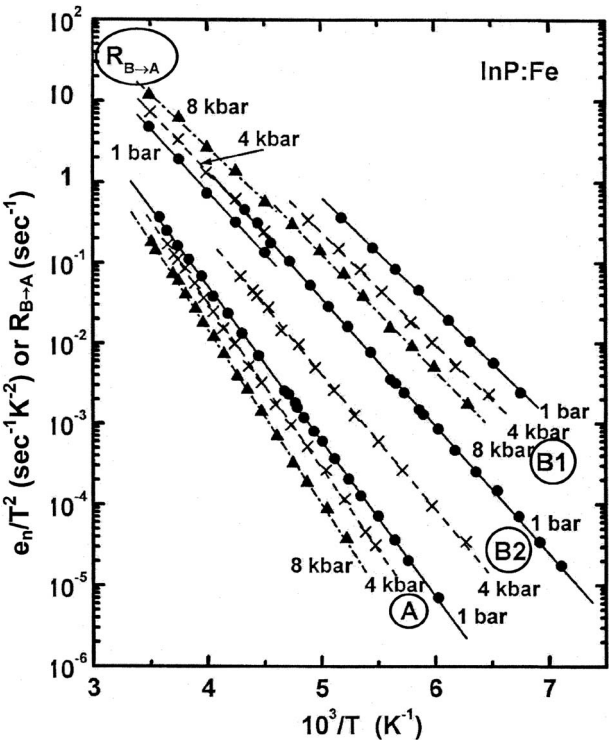


FIG. 4. Arrhenius plots of the electron emission rate, $e_n$ (plotted as $e_n/T^2$) for the $A$, $B1$, and $B2$ deep levels associated with the MFe center in InP and of the $B \to A$ transformation rate at different pressures. Note that the pressure effects on the $B2$ transition and the $B \to A$ transformation are opposite in sign.

preexponential $\Lambda$ in Eq. (3). The changes in $\Delta H_n$ are shown in Fig. 5. The emission enthalpy, $\Delta H_n = E_c - E_T$ (where $E_c$ is the conduction-band edge and $E_T$ is the deep level or trap energy below $E_c$), increases with pressure for all three levels, and the results in Fig. 5 show that the levels shift away from $E_c$ at rates of 5.9, 2.3, and 6.1 meV/kbar for the $A$, $B1$, and $B2$ levels, respectively, i.e., pressure shifts these levels deeper into the band gap.

In interpreting these results, it is important to note that electron emission is measured from the deep level to $E_c$, so that $E_c$ is the reference energy state relative to which $\Delta H_n$ and the change in $\Delta G_n$ are measured. However, this reference state is not fixed; it is pressure-dependent, and this dependence (represented by the hydrostatic deformation potential $\alpha_c$ of $E_c$, i.e., $\alpha_c \equiv \partial E_c/\partial \ln V$, where $V$ is the volume) contributes to the measured pressure dependence of $e_n$, and thereby to $(\partial \Delta G_n/\partial P)_T$. It is necessary to correct for this contribution in order to determine the absolute (i.e., relative to a fixed reference) shifts, $(dE_n/dP)_{\text{abs}}$ and $(\partial \Delta G_n/\partial P)_{T,\text{abs}}$, associated with emission. It is these shifts that contain the physics.

Several values of $\alpha_c$ for InP have been reported. Theoretical calculations have yielded values of $-5.04$ eV (Ref. 10) and $-5.9$ eV (Ref. 11) whereas a determination based on experimental results has yielded $-7.0$ eV.[12] For the present purposes we take $\alpha_c = -6.0 \pm 1.0$ eV and note that any reasonable uncertainty in this value will not materially affect the conclusions to be drawn later. When combined with a volume compressibility $K \equiv -(\partial \ln V/\partial P) = 1.38 \times 10^{-3}$/kbar,

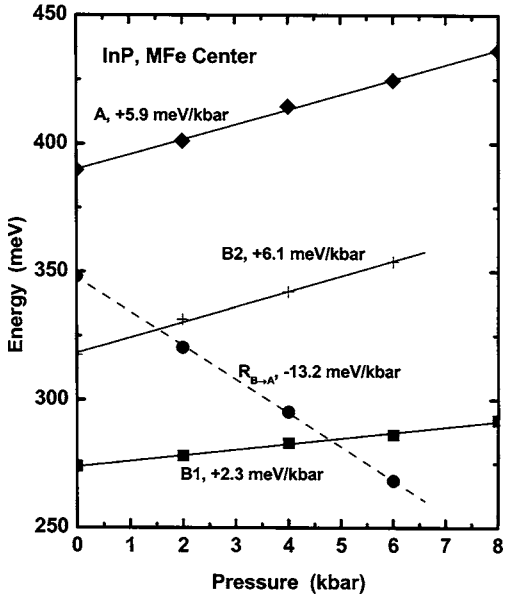


FIG. 5. Pressure dependences of the measured electron emission enthalpies, $\Delta H_n$, for the $A$, $B1$, and $B2$ deep levels of the MFe center in InP and of the enthalpy (or activation energy) for the $B \to A$ transformation. The enthalpy of the $B \to A$ transformation becomes the smallest energy of the problem above ~5 kbar.

this value of $\alpha_c$ yields $(dE_c/dP)_{\text{abs}} = +8.3 \pm 1.3$ meV/kbar for the absolute pressure shift of $E_c$.

It is of passing interest to compare this shift of $E_c$ with that of the direct gap ($E_g$) of InP. The experimental shift of the gap[13] is $dE_g/dP = d(E_c - E_v)/dP = 8.4 \pm 0.2$ meV/kbar, which implies that the absolute shift of the valence-band edge $E_v$ is $(dE_v/dP) = 0.1$ meV/kbar—a small value, i.e., the shift of the gap is largely determined by the shift of $E_c$.

With the above absolute pressure derivative of $E_c$ we can now determine the absolute pressure derivatives of the energies (or $\Delta H_n$'s) of the $A$, $B1$, and $B2$ levels from the measured derivative, namely $(dH_n/dP)_{\text{abs}} = (dH_n/dP)_{\text{meas}} - (dE_c/dP)_{\text{abs}}$. The deduced absolute pressure derivatives of $\Delta H_n$ for the three levels are given in Table I. The negative signs of these derivatives imply that these levels move closer with pressure to a higher-lying (i.e., higher in energy than the energies of the individual levels) fixed reference level.

Table I gives the 1 bar values of $\sigma_n$ (taken to be the infinite $T$ limit obtained from the intercepts of Arrhenius plots such as in Fig. 4) and its logarithmic pressure derivatives for the three deep levels. We note that the magnitudes of $\sigma_n$ are relatively large and comparable for the three levels, but we caution that the determination of $\sigma_n$ and its pressure derivative from the extrapolation of Arrhenius plots to infinite $T$ is fraught with uncertainty. We did not measure these properties directly.

Also given in Table I are the measured and absolute pressure derivatives of $\Delta G_n$. The measured derivatives were obtained directly from the measured $e_n(P)$ and $\sigma_n(P)$ via Eq. (6). We note that $(\partial \Delta G_n/\partial P)$ is temperature-dependent, but the results clearly show, as is generally true,[6] that this dependence is very weak. Consequently, the $(\partial \Delta G_n/\partial P)_{\text{meas}}$ in Table I is evaluated at 200 K, which is a representative $T$ in the middle of the range of the data (see Fig. 4). The absolute value of $(\partial \Delta G_n/\partial P)_T$ was evaluated from $(\partial \Delta G_n/\partial P)_{T,\text{meas}}$ by taking into account the absolute deformation potential of $E_c$ as discussed above.

Here we note that, from a thermodynamic point of view, the partial pressure derivative of $\Delta G_n$, i.e., $(\partial \Delta G_n/\partial P)_T$, is a volume change, $\Delta V^*$, which is an activation volume. In the absence of an activation capture barrier (or for a small barrier as assumed), $\Delta V^*$ can be interpreted as the breathing mode relaxation associated with the emission process. In dealing with defects and carrier emission or capture processes in semiconductors, we distinguish between two classes of lattice relaxations: symmetry conserving (or breathing mode) relaxation whereby the near-neighbor host atoms move inward or outward, and different types of symmetry breaking relaxations including the $D2h$ symmetry pairings that occur in the present case. This latter pairing relaxation describes the distortion of the nearest-neighbor atoms toward or away from each other within pairs. Hydrostatic pressure couples to the totally symmetric, or breathing mode, relaxation, so that the $\Delta V^*$ deduced from our measurements relates to this mode.

### E. Effect of pressure on the $B \to A$ transformation

The $B \to A$ transformation rate, $R_{BA}$, was obtained in the same manner as that used by Levinson *et al.*[2] Specifically, the $B2$ and $A$ peak heights were determined as a function of filling pulse width with the interval between pulses, $t_i$ (or pulse width PW), held constant. $R_{BA}$ was then determined using Eq. (1), in which $R_{AB}$ is taken as the $A$ emission rate at

TABLE I. Values of the emission enthalpies, $\Delta H_n$, and capture cross sections, $\sigma_n$, for the three deep levels of the MFe center and their pressure dependences. Also listed are the pressure dependences of $\Delta G_n$ and the activation volumes for the three emissions. $\Delta G_n$ is the change in free energy associated with the emission process. See text for details.

| Level | $\Delta H_n$ (meV) | $d\Delta H_n/dP$ (meV/kbar) meas. | $d\Delta H_n/dP$ (meV/kbar) abs. | $\sigma_n$ ($10^{-14}$ cm$^2$) | $d \ln \sigma_n/dP$ (% kbar) | $(\partial G_n \partial P)_T$ (meV/kbar) meas. | $(\partial G_n \partial P)_T$ (meV/kbar) abs. | $\Delta V^*$ (A$^3$/e) |
|---|---|---|---|---|---|---|---|---|
| $A$ | 391 | 5.9 | −2.4 | 1.8 | 11.0 | 5.8 | −2.5 | −4.0 |
| $B1$ | 27 | 2.3 | −6.0 | 2.9 | −8.4 | 2.4 | −5.9 | −9.4 |
| $B2$ | 317 | 6.1 | −2.2 | 1.5 | −19.8 | 6.2 | −2.1 | −3.3 |

the peak temperature, since electron emission from $A$ controls this latter rate.

The results for $R_{BA}$ are shown in Fig. 4, which also compares this transformation rate with the $B2$ emission rate. A very important aspect of this comparison is the fact that the effects of pressure on $R_{BA}$ and the $B2$ emission rate are opposite; the former increases and the latter decreases with pressure at any fixed temperature. Additionally, the 1 bar curve for $R_{BA}$ does not coincide with the 1 bar curve for the $B2$ emission. These results suggest that, in contrast with Levinson *et al.*'s conclusion based only on 1 bar data,[2] the $B2$ electron emission process and the $B \rightarrow A$ transformation process are not controlled by the same barrier, i.e., they do not proceed by the same mechanism.

The striking difference between $B \rightarrow A$ transformation and the $B2$ emission process is also seen in the comparison of the pressure dependence of their activation energies shown in Fig. 5. Whereas $E_{B2}$ *increases* at a rate of 6.1 meV/kbar, $E_{B \rightarrow A}$ *decreases* at a rate of 13.2 meV/kbar. As is clear from the results in Fig. 5, the rapid decrease in $E_{B \rightarrow A}$ with pressure makes this activation energy above ~5 kbar the smallest of the various activation energies in the MFe center problem, and this is why the center prefers the $A$ configuration at high pressure.

The coincidence of the Arrhenius plots for the $B2$ electron emission and the $B \rightarrow A$ transformation observed by Levinson *et al.*[2] at atmospheric pressure led them to conclude that these processes were identical and formed the basis of their model. We have explored this issue in more detail. Recall that, as shown in Fig. 4, the Arrhenius curve for $B2$ emission does not coincide with that for the $B \rightarrow A$ transformation. However, if we do not include the $T^2$ temperature variation in the prefactor for the $B2$ emission (as done by Levinson *et al.*), and plot $e_n$ rather than $e_n/T^2$, the curves nearly coincide at 1 bar as shown in Fig. 6. (Of course this near coincidence occurs only at 1 bar.) Plotted in this fashion, the results agree with those of Levinson *et al.*[2] However, we do not believe that this is the appropriate presentation of the data. Levinson *et al.*[2] argue that the $B2$ emission is not a simple electron-capture–emission process in equilibrium with the conduction band and thus should not contain the $T^2$ dependence. However, our results indicate that the $B2$ emission is not the same as the $B \rightarrow A$ transformation rate even at 1 bar, as shown.

We have followed Levinson *et al.*[2] in obtaining additional experimental results for the $B \rightarrow A$ transformation rate at low temperature. This was done by cooling the sample under bias so that all the MFe centers were in the $B$ configuration, and then turning the bias off for a given known time. TSCAP was then measured under bias to determine the fraction of defects that had converted to the $A$ configuration. These additional data are shown in Fig. 6 along with the $B2$ emission rate data uncorrected for the $T^2$ dependence. Again we emphasize the opposite trends in these data as pressure is increased, leading to the conclusion that these two processes are not due to the same physical mechanism.

### F. Additional results on the bistability of the MFe center

Most of the experimental data presented thus far were obtained by performing the complete measurement at a given constant pressure. In order to further explore the pressure-dependent behavior of the MFe bistability, we also performed some experiments where the pressure was varied during the measurement. For example, in one case the sample was cooled at 1 bar with the bias on so that at 80 K all the centers were in the $B$ configuration. The $B$'s were then filled at 80 K (with 2 $\mu$s filling pulse), and the pressure was then raised at 80 K to 8 kbar and held for 10 min (these two steps, i.e., the trap filling and raising of the pressure were also reversed with no difference in outcome). The pressure was then lowered back to 0 kbar, and TSCAP was performed (at a heating rate of a few degrees K/min) with the result that all the centers were found to be in the $B$ configuration. This result indicates that the transformation from $B$ to $A$ cannot be brought about at 80 K merely by raising the pressure to 8 kbar. The fact that this transformation process must still be thermally activated at 8 kbar agrees qualitatively with the data in Fig. 5, which, when extrapolated to 8 kbar, suggest that the activation energy for $B \rightarrow A$ is still greater than 0.2 eV at 8 kbar.

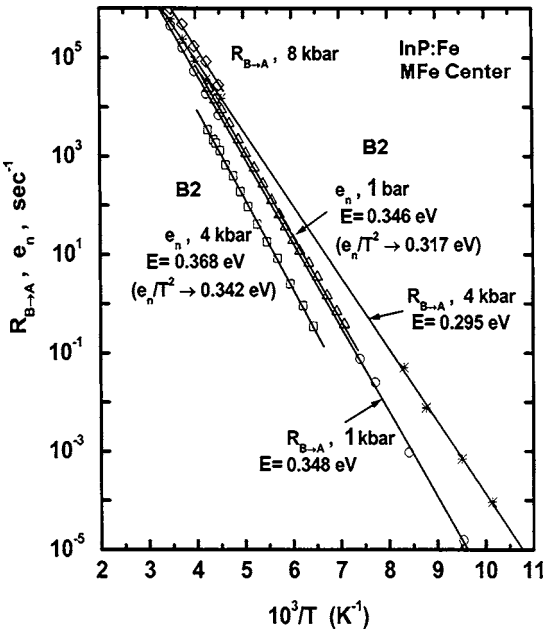


FIG. 6. Arrhenius plots of the $B \rightarrow A$ transformation rate and of the $B2$ emission rate, $e_n$ (without the $T^2$ connection), showing that whereas the $B \rightarrow A$ rate and the $B2$ emission plots are nearly indistinguishable at 1 bar, they exhibit opposite pressure dependences definitively showing that the two rates do not represent the same process.

The above experiment was repeated with the pressure held at 8 kbar after raising it to this level at 80 K. The measurement of TSCAP at 8 kbar revealed that nearly all the centers were in the $A$ configuration, with only a very small step observed corresponding to $B$ emission. It is important to realize that at the start of the TSCAP measurement all of the centers are in the $B$ configuration. This result suggests that at high pressures the $B \rightarrow A$ transformation can be accomplished without electron emission from the $B$ states. Such a process would not fit with the model proposed by Levinson *et al.*,[2] but, as we have concluded, the $B2$ electron emission

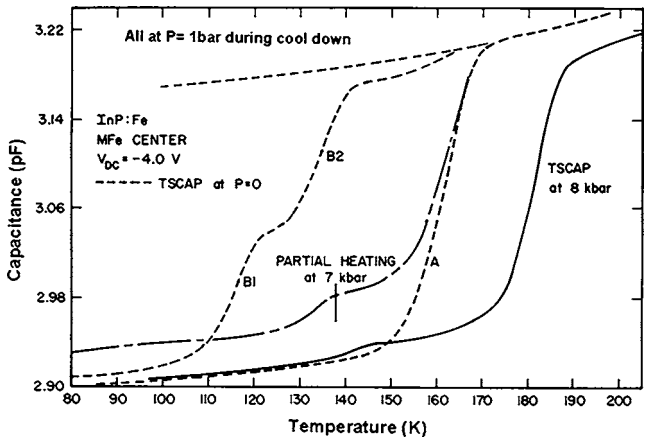


FIG. 7. TSCAP spectra of the *A* and *B* configurations of the MFe center showing that starting in the *B* configuration, partial heating of the sample to ~140 K at 7 kbar followed by cooling back to 80 K and releasing the pressure to 1 bar results in largely the *A* configuration. See text for details of this experiment. Repeating this sequence of steps at 1 bar yields the *B* configuration.

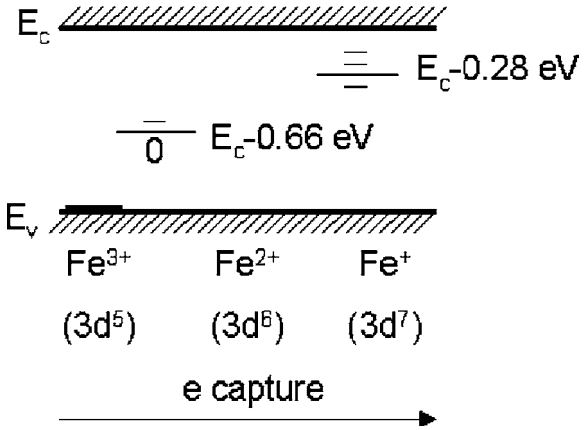


FIG. 8. Energy level diagram for the various charge states of substitutional Fe in InP according to Ref. 14.

and $B \rightarrow A$ transformation mechanisms are different, even though they are both thermally activated. This result is also not unexpected when one observes that, according to the data in Fig. 5, at 1 bar the $B \rightarrow A$ activation energy is greater than the emission energies for both $B1$ and $B2$, but that at 8 kbar just the opposite is true: the $B \rightarrow A$ activation energy is less than the *B* emission energies. This comparison indicates that under the right conditions (high pressure in our case), the $B \rightarrow A$ transformation may be brought about without *B* electron emission.

The above results prompted the performance of a third experiment in which the sample was partially heated at high pressure, cooled back down to 80 K, and at that point the pressure was taken down to 1 bar and then the TSCAP measurement was made. The result for this experiment is shown in Fig. 7 along with results for constant pressure during the entire experiment. The specifics of this experiment are as follows: subsequent to filling the *B* traps at 80 K, the pressure was raised to 7 kbar, and the sample was heated at this pressure to just under 140 K (vertical line in Fig. 7). The temperature was then lowered back to 80 K with the pressure maintained at 7 kbar. Finally, the pressure was lowered to 1 bar and the TSCAP measurement was made resulting in the long/short dashes curve shown in Fig. 7. If this entire sequence had been performed at 1 bar, the result would have been a recovery of the capacitance to nearly that for the baseline equilibrium value due to $B1$ and $B2$ electron emission during the partial heating step. However, the pressure sequence used resulted in significant conversion to the *A* configuration. We suggest that the temperature of 140 K was insufficient to cause significant *B* electron emission at 7 kbar, but was sufficient to provide the thermal energy required to cause the $B \rightarrow A$ conversion at 7 kbar. At 7 kbar, the $B \rightarrow A$ activation energy becomes the smallest activation energy among the various transitions involved (see Fig. 5) and significant activation occurs at 140 K. Thus, like the opposite variations of the *B* emission energies and the $B \rightarrow A$ activation energy with pressure, this result decouples the physical process responsible for *B* electron emission from that responsible for conversion from the *B* to the *A* configuration.

### G. Atomic models for the MFe center

In exploring possible models for the MFe center in InP, it is necessary to recall that (i) the center is only found in Fe-doped InP, and therefore it is Fe-related; and (ii) it is found in $p^+/n$ junction devices and not in Schottky devices made from the same material; therefore, it involves a processing-induced defect.[2] The crucial junction processing step is the high temperature diffusion of either Zn or Cd to form the $p^+$ region. These factors hold important clues as to the atomic configurations of MFe.

Iron is known[14] to be a substitutional double acceptor on the In site in InP. The dominant Fe species is the neutral substitutional $Fe^0_{In}$ (corresponding to $Fe^{3+}$ i.e., the $3d^5$ ion) with electronic level at the top of the valence band (Fig. 8). The first acceptor level (−/0) is located at $E_c$-0.66 eV, i.e., at midgap, pinning the Fermi level and responsible for the semi-insulating properties of Fe-doped InP. The (−/0) transition corresponds to $Fe^{2+} \rightarrow Fe^{3+}$ (or $3d^6 \rightarrow 3d^5$). It is not involved in MFe, and we did not observe it because we did not go to sufficiently high temperature. The second acceptor level (=/−) is located at $E_c$-~0.28 eV and corresponds to the $Fe^{+} \rightarrow Fe^{2+}$ (or $3d^7 \rightarrow 3d^6$) transition. The energy of this transition is essentially identical to that of the $B1$ transition of MFe ($E_{B1}$=0.27 eV) leading to the suggestion by Wager and Van Vechten[7] that $B1$ is the (=/−) transition of substitutional Fe.

#### *1. Model I*

Wager and Van Vechten[7] have made two observations leading to a proposed atomic Model I for MFe. The first is that $p^+$ doping by substituting a group II element, Zn or Cd, for the group III element In greatly increases the concentration of *P* vacancies ($V_P$) in the $p^+$ region. Some of these vacancies come out of the adjoining *n* region and thereby cause the concentration of In vacancies ($V_{In}$) in this region to increase so as to maintain Schottky equilibrium. The second

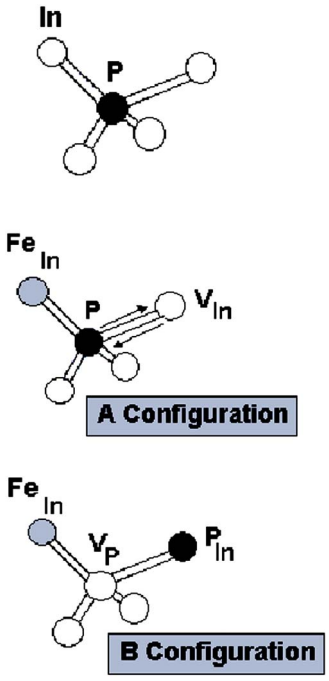


FIG. 9. (Color online) Atomic configurations of the InP and P atoms in InP and of the $A$ and $B$ configurations of MFe center according to Model I described in the text. A nearest-neighbor hop of the P atoms into the site of the In vacancy ($V_{\mathrm{In}}$) results in transforming the MFe center from the $A$ to the $B$ configuration.

observation is that an important mechanism for diffusion in III-V semiconductors is near-neighbor (NN) anion hopping. Thus, In vacancies in the $n$ region diffuse by NN $P$ hopping leading to the formation of $V_P$'s and $P$ antisites ($P_{\mathrm{In}}$'s) according to the reaction $V_{\mathrm{In}} \underset{\mathrm{NN}P\mathrm{hop}}{\rightleftarrows} V_{\mathrm{P}}+P_{\mathrm{In}}$, which is illustrated in Fig. 9. Thus, according to Model I, in the $n$ region, which is probed by the present DLTS and TSCAP experiments, the following defect species should be present simultaneously: $\mathrm{Fe}_{\mathrm{In}}$, $V_P$, $V_{\mathrm{In}}$, and $P_{\mathrm{In}}$. Noting that $E_{B2}$ is close to the energy of the (0/+) transition of the $V_P$ (=0.36 eV),[7,15] Wager and Van Vechten[7] proposed a model in which $V_P$ is part of the structure of MFe.

According to Model I, the $A$ atomic configuration is the complex $\mathrm{Fe}_{\mathrm{In}}\mathrm{V}_{\mathrm{In}}$. After a DLTS filling pulse at low temperature, the stable $A$ configuration becomes $\mathrm{Fe}_{\mathrm{In}}^{-}\mathrm{V}_{\mathrm{In}}^{-}$, corresponding to the $\mathrm{Fe}^{2+}$, or $3d^6$, ion, i.e., the capture of one electron. A small capture cross section for this center apparently precludes $\mathrm{Fe}_{\mathrm{In}}$ from capturing a second electron. The $A \rightarrow B$ transition, represented by the $A$ transition in TSCAP (see Fig. 1) involves a NN $P$ hop and can be represented as

$$\mathrm{Fe}_{\mathrm{In}}^{-}V_{\mathrm{In}}^{-} \underset{\mathrm{capture}}{\overset{\mathrm{emission}}{\rightleftharpoons}} \mathrm{Fe}_{\mathrm{In}}^{-}V_{\mathrm{P}}^{+}P_{\mathrm{In}}^{+}+3e.$$

Thus, the $B$ configuration is a complex involving $\mathrm{Fe}_{\mathrm{In}}$, $V_P$, and $P_{\mathrm{In}}$. By assuming that $V_P^+$ and $P_{\mathrm{In}}^+$ are the normal ionization states of $V_P$ and $P_{\mathrm{In}}$, Model I indicates that this transition involves the emission of three electrons.

On cooling this $B$ configuration in the absence of free electrons (i.e., under reverse bias) and then zero biasing, the stable $B$ configuration at low temperature becomes $\mathrm{Fe}_{\mathrm{In}}^{2-}V_{\mathrm{P}}^{0}P_{\mathrm{In}}^{+}$, corresponding to the $\mathrm{Fe}^{+}(3d^7)$ configuration of $\mathrm{Fe}_{\mathrm{In}}$. The $B1$ transition is associated with the (=/−), or $\mathrm{Fe}^{+}(3d^7)$ to $\mathrm{Fe}^{2+}(3d^6)$ transition of $\mathrm{Fe}_{\mathrm{In}}$ and can be represented by

$$\mathrm{Fe}_{\mathrm{In}}^{2-}V_{\mathrm{P}}^{0}P_{\mathrm{In}}^{+} \xrightarrow{\mathrm{Fe}_{B1}} \mathrm{Fe}_{\mathrm{In}}^{-}V_{\mathrm{P}}^{0}P_{\mathrm{In}}^{0}+1e.$$

The $B2$ transition is the (0/+) transition of $V_P$ and can be represented as

$$\mathrm{Fe}_{\mathrm{In}}^{-}V_{\mathrm{P}}^{0}P_{\mathrm{In}}^{+} \xrightarrow{E_{B2}} \mathrm{Fe}_{\mathrm{In}}^{-}V_{\mathrm{P}}^{+}P_{\mathrm{In}}^{+}+1e.$$

It should be cautioned here that the model assumes the above charge states for the various defects and does not consider or rule out alternative states. Furthermore, the normal ionization state of $P_{\mathrm{In}}$ is assumed to be $P_{\mathrm{In}}^+$ whereas more recent first-principles calculations (see below) show this state to be $P_{\mathrm{In}}^0$ under $n$ conditions. Thus, there are serious concerns about the assumptions of Model I.[16]

We now examine this Model I in light of both the high pressure results presented earlier in the paper and first-principles results on native defects in InP.

A number of authors have employed parameter-free first-principles *ab initio* methods to calculate the formation energies and energy levels for the various charge states of vacancies and antisites in InP.[17–19] The calculations differ in the size of the basis sets used that determine the accuracy and in the types of the pseudopotentials. Jensen[17] employed 32-atom supercells and omitted lattice relaxations. Seitsonen *et al.*[18] improved the accuracy by using 64-atom supercells and included lattice relaxations. More recently, Castleton and Mirbt[19] went further by using a series of supercells up to 512 atoms, included lattice relaxations, and assessed errors coming from the size of the supercells.

In the discussion to follow, we want to compare the appropriate results from these calculations, primarily the breathing mode relaxations, to our results from the pressure experiments. In doing so, the reader is again cautioned that the calculations are for simple isolated defects in InP whereas the defects associated with the MFe center according to Model I are more complex. Additionally, we discuss the MFe defect levels in terms of the degeneracies and symmetries of the isolated defects. There is no justification for doing so other than the hope that the distortions and energy level splittings (if present) of the defects in Model I are relatively small. Thus, we seek mainly qualitative agreement with the hope of gaining some insight about the model. In view of this objective, we choose to compare to the breathing mode relaxations of Seitsonen *et al.*[18] listed in Table II as they are more complete than those of Castleton and Mirbt.[19] Inaccuracies due to supercell size for cells >64 atoms are not of primary concern for our purposes, and in any case they can be assessed. In Table II the pairing mode relaxation describes the deviations from the purely radial (breathing mode) relaxation. Specifically, it describes the distortion of the nearest neighbors toward (−) or away from (+) each other within two pairs.

TABLE II. The nearest-neighbor relaxation components for the different charge states of the defects in InP thought to be involved in the *A* and *B* configurations of the MFe center. The amplitudes are given in percent of the bulk bond distance of InP. A negative breathing mode relaxation implies inward relaxation. After Seitsonen *et al.*, Ref. 18.

| Defect | Breathing | Pairing |
|---|---|---|
| $V_{\mathrm{In}}^{0}$ | −16.1 | 2.0 |
| $V_{\mathrm{In}}^{-}$ | −14.9 | 2.7 |
| $V_{P}^{+}$ | −5.5 | 0 |
| $V_{P}^{0}$ | −13.2 | 9.0 |
| $P_{\mathrm{In}}^{+}$ | −6.0 | 0 |
| $P_{\mathrm{In}}^{0}$ | −3.3 | 0 |

*a. B1 Transitions*. In the double acceptor, i.e., the (=) $Fe^{+}(3d^{7})$, or $Fe_{In}^{2-}$, state of $Fe_{In}$, the second captured electron goes into an antibonding-like state. Compression of the lattice should raise this level higher in the gap and this is what we observe: the absolute shift of $E_{B1}$ (relative to a higher-lying reference state) being −6.0 meV/kbar (see Table I). Additionally, electron capture into an antibonding level should cause the NN atoms to relax outward due to repulsion. Subsequent emission of the captured electron (i.e., the the =/− transition) should lead to inward relaxation of the same magnitude. This is indeed what we find, namely $\Delta V^{*}=-9.4\ \mathrm{A}^{3}/e$ for this transition, a large inward relaxation that favors the *A* configuration.

*b. B2 transitions*. According to the Model I, the *B*2 transition is presumed to be the (0/+) transition of $V_P$. Considerable knowledge exists about vacancies in III-V semiconductors. On forming such vacancies, the dangling $sp^{3}$ orbitals hybridize to form bonding and antibonding states. The bonding states, which are *s*-like in character, belong to the nondegenerate $A_1$ representation and are resonant in the valence band. The antibonding states, which have *p*-like character, on the other hand, belong to the threefold degenerate $T_2$ representation and form deep levels in the gap.

On forming $V_P^0$ in InP, five valence electrons are removed leaving three, two of which go into the $A_1$ level and the remaining electron goes into $T_2$. Being antibonding, the $T_2$ level rises in the gap on compression, and this is what we observe, namely the absolute shift of $E_{B2}$ (relative to a higher-lying reference state) is −2.2 meV/kbar. The presence of the electron in $T_2$ can also be expected to cause outward relaxation of the near neighbors. Emission of the electron associated with the (0/+) transition should thus produce the opposite effect, i.e., inward relaxation. Again, this is what we observe, namely $\Delta V^{*}=-3.3\ \mathrm{A}^{3}/e$ for this transition.

This result appears to be at odds with Seitsonen *et al.*'s calculations,[18] and this is one of the problems for Model I. These authors obtained an inward breathing relaxation on forming $V_P^+$ of $\Delta r=-5.5\%$, where *r* is the bulk bond distance of InP. In this charge state the $T_2$ state is empty and $V_P^+$ has its undistorted $T_d$ symmetry. On forming $V_P^0$, however, there is an inward breathing mode relaxation of $\Delta r=-13.2\%$ and a nearest-neighbor outward pairing relaxation of +9.0%. Considering only the breathing mode relaxations, these results suggest an outward relaxation of $\Delta r=-5.5\%-(-13.2\%)=+7.7\%$ on electron emission, an effect that is opposite in sign from what we deduce from the pressure experiments. It should be pointed out, however, that while in the MFe complex $V_P$ does not have tetragonal symmetry and a $T_2$ level, it is a full bond length away from the next defect and hopefully the additional level splitting is not too large. Additionally, there is the large positive pairing relaxation associated with $V_P^0$ indicating a large local distortion that can negate our comparison for this defect

*c. The A→B transition*. As noted above, the net effect of this transition is the transformation of $V_{\mathrm{In}}^{-}$ into a $V_P^+P_{\mathrm{In}}^+$ pair via a NN *P* hop. The fact that pressure favors the *A* (i.e., $V_{\mathrm{In}}^{-}$) configuration implies that the $V_{\mathrm{P}}^+P_{\mathrm{In}}^+$ pair has a larger volume than $V_{\mathrm{In}}^{-}$. This conclusion is consistent with Seitsonen *et al.*'s[18] results in Table II, as can be roughly seen by comparing the inward breathing mode relaxation for $V_{\mathrm{In}}^{-}$ with the sum of the relaxation for $V_{\mathrm{P}}^+P_{\mathrm{In}}^+$. A favorable aspect in this regard relevant to our pressure results is that the dominant relaxations for $V_{\mathrm{In}}^{-}$, $V_P^+$, and $\mathrm{P}_{\mathrm{In}}^+$ are breathing mode relaxations with only $V_{\mathrm{In}}^{-}$ exhibiting a rather small pairing relaxation.

The neutral In vacancy, $V_{\mathrm{In}}^{0}$, has two electrons in the $A_1$ state and three electrons in $T_2$ levels in the gap. On forming $V_{\mathrm{In}}^{-}$, the captured electron pairs with the third electron in the higher $T_2$ antibonding level, producing what we expect to be a smaller relaxation than that obtained for $V_{\mathrm{In}}^{0}$. This is confirmed by Seitsonen *et al.*'s results[18] in Table II. It is seen that on forming $V_{\mathrm{In}}^{0}$ ($V_{\mathrm{In}}^{-}$), $\Delta r=-16.1\%\,(-14.9\%)$, i.e., there is an outward (inward) relaxation on electron capture (emission). Thus, pressure would favor the empty state of the *A* configuration of MFe.

Finally, in forming $P_{\mathrm{In}}^{0}$, the extra two electrons from the *P* fill the antibonding $A_1$ state, which lies deep in the gap.[18] Electron emission yields $P_{\mathrm{In}}^{+}$ with one electron in $A_1$. The calculated breathing mode relaxations (there are no pairing distortions) given in Table II are $\Delta r=-6.0\%$ (−3.3%) for $P_{\mathrm{In}}^{+}(P_{\mathrm{In}}^{0})$, respectively. Thus, there is an outward (inward) relaxation of $|\Delta r|=2.7\%$ on electron capture (emission) for this defect, as we would intuitively expect for an antibonding level. This means that pressure would favor the $P_{\mathrm{In}}^{+}$ state over the $P_{\mathrm{In}}^{0}$ state in the absence of other defects; but this is not the case for the *B* configuration of MFe, which also involves $Fe_{In}$ and $V_P$.

### *2. Model II*

Because Model I involves the transfer of three electrons (as we discussed earlier) and Levinson *et al.*[2] suggested only two electrons were transferred, Wager and Van Vechten[7] proposed an alternative model (II) for the MFe center. In this case, the *A* configuration in its electron occupied state is a bond-center interstitial configuration, $Fe_{bc}^{-2}$, and the *B* configuration is $Fe_{In}^{-}V_{\mathrm{P}}^{+}$. The authors went on to suggest that experiments at high pressure should distinguish between the two models. Specifically, it was thought that pressure should

favor the $B$ configuration for Model I because the repulsion between $Fe_{In}^{-}$ and $V_P^{-}$ in the $A$ configuration would lead to expansion of the lattice (opposed by pressure). But, if Model II were correct, then the $A$ configuration should be favored due to the contraction of the lattice about the $Fe_{bc}$. Clearly this view for Model I is contradicted by our pressure results, which unambiguously show that pressure stabilizes the $A$ configuration at the expense of $B$. And while our pressure results do not necessarily rule out Model II, there is the significant issue of how to contend with the additional defects produced by the In and P atoms generated in the $Fe_{bc} \rightarrow Fe_{In} V_P$ transformation in this model.

## IV. CONCLUDING REMARKS

The main results of the present work can be summarized as follows.

(i) Hydrostatic pressure has a drastic influence on the energetics and kinetics of the various processes associated with the MFe center. The energies and their pressure dependences as well as the activation volumes ($\Delta V^{*}$) for these processes were determined. In the absence of barriers to electron capture, or for small barriers, $\Delta V^{*}$ can be interpreted as the breathing mode relaxation associated with electron emission or capture.

(ii) By 8 kbar, the $A$ configuration is stabilized regardless of bias conditions during cooling because at these pressures the $B \rightarrow A$ transition energy becomes the smallest energy of the problem.

(iii) While the $A \rightarrow B$ transformations appear to be charge state controlled at 1 bar, this is not so at high pressure.

(iv) A speculative atomic model (I)[7] for the MFe center was discussed. Several features of the model, including the breathing mode relaxations associated with the various electron emissions, are consistent with the experimental results, but some issues remain.

(v) An alternative atomic model (II)[7] was mentioned briefly but is not supported by the pressure results.

(vi) While the experimental results favor a model that involves the emission of two electrons in the $A \rightarrow B$ transformation, the issue of whether two or three electrons are involved is still not completely resolved experimentally.

As for the comparison with first-principles results we made in Sec. III G, we emphasize here again that these results are for isolated defects in InP, and the calculated formation energies[17–19] for the various charge states of these defects do not favor some of the species in model I of MFe, which is a complex center. Nevertheless, we found this comparison useful at least with respect to the sign of the breathing mode relaxations.

Finally, while our pressure results do not constitute a proof of Model I, they are generally consistent with some of its features, a finding that suggests that the model might serve as a starting point for the development of a more definitive model for this interesting center, the MFe in InP.

## ACKNOWLEDGMENTS

We are indebted to Mark Levinson for providing the samples quite some time ago, and to Len Hansen for technical assistance. Sandia is a multiprogram laboratory operated by Sandia Corporation, a Lockheed Martin Company, for the U.S. Department of Energy under Contract No. DE-A-94AL85000. The work done at the Jet Propulsion Laboratory, California Institute of Technology, was performed under a contract with the National Aeronautics and Space Administration.

[1] M. Levinson, M. Stavola, J. L. Benton, and L. C. Kimerling, Phys. Rev. B **28**, 5848 (1983); See also M. Levinson, J. L. Benton, and L. C. Kimerling, *ibid.* **27**, 6216 (1983).

[2] M. Levinson, M. Stavola, P. Besomi, and W. A. Bonner, Phys. Rev. B **30**, 5817 (1984); J. Electron. Mater. **14a**, 1133 (1985).

[3] G. E. Jellison, Jr., J. Appl. Phys. **53**, 5715 (1982).

[4] S. K. Bains and P. C. Banbury, J. Phys. C **18**, L109 (1985).

[5] G. M. Martin and S. Makram-Ebeid, in *Deep Centers in Semiconductors*, edited by S. T. Pantelides (Gordon and Breach, New York, 1986), p. 399.

[6] G. A. Samara, D. W. Vook, and J. F. Gibbons, Phys. Rev. Lett. **68**, 1582 (1992), and references therein; see also G. A. Samara, Phys. Rev. B **39**, 12764 (1989), and references therein; A preliminary report on the present work was presented at the 10th International Conference on High Pressure in Semiconductor Physics and published in the proceedings [Phys. Status Solidi B **241**, 3293 (2004)].

[7] J. F. Wager and J. A. Van Vechten, in *Microscopic identification of Electronic Defects in Semiconductors*, edited by N. M. Johnson, S. G. Bishop, and G. D. Watkins, Materials Research Society Symposia Proceedings No. 46 (MRS, Pittsburgh, 1985), p. 325; see also Phys. Rev. B **32**, 5251 (1985).

[8] The samples were kindly provided years ago by Dr. Mark Levinson, then of AT&T Bell Laboratories, and were from the same batch of devices used by Levinson and colleagues in their work (Ref. 2 above).

[9] G. D. Pitt, J. Lees, R. A. Hoult, and R. A. Stradling, J. Phys. C **6**, 3283 (1973); G. D. Pitt, Solid State Commun. **8**, 1119 (1970).

[10] C. G. Van de Walle, Phys. Rev. B **39**, 1871 (1989).

[11] M. Cardona and N. E. Christensen, Phys. Rev. B **35**, 6182 (1987).

[12] D. D. Nolte, W. Walukiewicz, and E. E. Haller, Phys. Rev. Lett. **59**, 501 (1987).

[13] H. Müller, R. Trommer, M. Cardona, and P. Vogl, Phys. Rev. B **21**, 4879 (1980).

[14] S. Fung, R. J. Nicholas, and R. A. Stradling, J. Phys. C **12**, 5145 (1979).

[15] H. Temkin, B. V. Dutt, and W. A. Bonner, Appl. Phys. Lett. **38**, 431 (1981).

[16] We hasten to add, however, that Model I and Model II are tentative suggestions proposed in a relatively short paragraph. As far as we know, there are no other models for MFe center.

[17] R. W. Jansen, Phys. Rev. B **41**, 7666 (1990).

[18] A. P. Seitsonen, R. Virkkunen, M. J. Puska, and R. M. Nieminen, Phys. Rev. B **49**, 5253 (1994).

[19] C. W. M. Castleton and S. Mirbt, Physica B **340–342**, 407 (2003); Phys. Rev. B **70**, 195202 (2004).